

Parametric Modelling of Biomimetic Propulsion Systems for Underwater Vehicles

Biali F. Lima Rodríguez, Edisson A. Naula, Ciro A. Rodríguez, and J. Israel Martínez López*
 Tecnológico de Monterrey, Avenida Eugenio Garza Sada Sur 2501, Monterrey, Mexico
 Email: A00831365@itesm.mx, A00825462@itesm.mx, ciro.rodriguez@tec.mx, israel.mtz@tec.mx

Abstract— In this work, a novel pseudorandom algorithm for generating in-silico biomimetic models of caudal fins for additive manufacturing for flexible materials is presented. The methodology provides a tool to develop caudal fin models for different morphologies (within rounded, truncated, forked and lunated), geometrical features and, considering randomness to improve the lifelikeness of the model. The algorithm’s capability to generate designs with customized hydrodynamic features was evaluated in-silico using computational fluid dynamics comparing the maximum velocity and the angle of attack. Numerical data shows that customization of key dimensional can be integrated into a flexible and dynamic design process. This capability is a step forward to emulate the robustness and adaptative nature of evolution.

Index Terms—generative design, parametric design, biomimetic, underwater vehicle, visual programming language, additive manufacturing.

I. INTRODUCTION

Additive Manufacturing (AM) is the processing method of joining materials by applying material layer upon layer to create pieces from 3D model data [1]. Unlike conventional manufacturing that relies on the removal of materials, AM makes three-dimensional pieces by adding materials layers in a regulated manner. This approach can save raw materials generating less waste [1]–[4]. AM has shifted in the last decades from prototyping to manufacturing customized functional parts. Automotive, aerospace, machinery, electronics, and medical products industries employ these advantages for testing new strategies or manufacturing parts considering a particular patient or client [5].

Underwater vehicles and Autonomous Underwater vehicles (UAVs) are vehicles capable of submerging in the water and operating for marine research, coastal security, underwater archeology, and surveillance of electrical or petrochemical underwater infrastructure [6].

Biological organisms are highly effective in solving problems, and nature has provided them with strategies and designs to survive in adverse underwater conditions [7]. UAVs are required to operate in highly diverse and harsh environments. Inspiration from nature can help overcome limitations and solve problems that traditional

propulsion systems have, such as poor maneuverability and loud operation of propellers [6].

Ideally, the navigation, sampling, and biosensing on the underwater Point-of-Care should be developed efficiently without significant disruptions of flora and fauna. However, in reality, the incursion of these devices can potentially injure fish or remove them from their natural habitat [8]. Hence, research of a new generation of UAVs with more natural features that mimic fauna can provide less disruptive and efficient designs.

Inspection of the manufacturing methodologies of recent developments shows that the impact of AM has been modest for biomimetic developments. Considering the capacity of resin-based additive manufacturing processes such as stereolithography to create pieces with features such as high-temperature resistance and high flexibility can enhance the recreation of undulating locomotion of animals such as fishes, snakes, or salamanders.

Table I shows a selection of recent research work on the implementation of biomimetic propulsion systems. It is noticeable that various types of materials employed that match a diverse array of requirements and employed materials.

TABLE I. MATERIALS ON DIFFERENT BIOMIMETIC PROPULSION SYSTEMS

Authors	Reference	Material
A. Apalkov et al.	[8]	Polyester and two different types of flexible plastic were used to make center plates and reinforcing ribs.
S. Heo et al.	[9]	Polypropylene (PP) Plastic Sheet
L. Junqiang et al.	[10]	Aluminum Alloy 1106 (Al-1106)
T. Salum ä et al.	[11]	Mold Silicon (Si)
T. Wang et al.	[12]	Carbon Fiber Reinforced Polymer (CFRP)
P. Riggs et al.	[13]	Silicone Rubber Resin (VMQ)
A. D. Marchese et al.	[14]	Polyoxymethylene (POM)
M. Ay et al.	[15]	Mold Silicon (Si)
C. T. Aparicio-Garc á et al.	[16]	Polydimethylsiloxane (PDMS) and Poly(lactic Acid Filament (PLA) , Thermoplastic Polyurethane (TPU)

Besides the material, the shape of the fin is a key parameter to be considered. Variation of the design parameters on the caudal fin is presented (Table II) to

Manuscript received July 15, 2021; revised November 30, 2021.
 Corresponding author: J. Israel Martínez López (israel.mtz@tec.mx)

find which are the key parameters to achieve better performance depending on the goal and purpose of the component (Fig 1).

TABLE II. CAUDAL FIN PARAMETERS STATE-OF-ART

Work Document	Reference	Material on the propulsion system
A. Apalkov et al.	[8]	Variation of the elasticity on the caudal fin
S. Heo et al.	[9]	Thickness variation
P. Riggs et al.	[13]	Comparison of a biomimetic fin vs an NACA airfoil
A. Krishnadas et al.	[17]	Caudal peduncle, leading edge, trailing edge

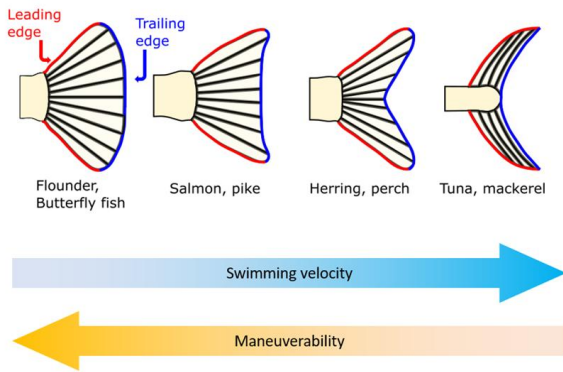


Figure 1. Swimming velocity and different types of fins.

Recently parameters on caudal fins has been tested to know which caudal fin-type will show better results in their performance, maximizing thrust, reduce the power consumption and noise generated.

Several kinds of parameters have been assessed, such as the frontal shape, differing the fin’s leading edge and the trailing edge [17], the foil of the fin, e.g., varying the thickness of the caudal fin [9] or comparing a biomimetic fin with a NACA foil [13] also the same shape but with different materials i.e., varying the elasticity of the caudal fin [8].

The thrust is produced considering the force produced due to the pressure distribution across the surface from the interaction of the tail with the fluid around. Typically the distribution will be produced accordingly to the animal swimming velocity and maneuverability (see Fig. 1).

The relationship of the overall shape has a relevant role on the performance of these propulsion systems. For example, according to Sfakiotakis et al. [7] the aspect ratio of the caudal fin for thunniform swimmers can be defined in a range from 4.5 to 7.2 with aspect ratio shown in the Equation 1. The aspect ratio (AR) is defined as the fin span (b) squared, divided by the projected fin area (Sc) (see Equation 1),

$$AR = b^2 / Sc \tag{1}$$

To the best of the authors’ knowledge, there are no reported systematic studies of generative designs for underwater vehicles. In this work, we propose the parametric design of flexible caudal fins that could be

implemented for additive manufacturing in the future. As a proof-of-concept, we propose evaluating in-silico of caudal fins with contrasting features to show the potential to produce designs with tunable features.

Swimming involves several forces between the fish and the surrounding water, such as lift and drag.

The viscous swimming drag (D_F) depends on the wetted area and the speed that the fish has [7], and it can be calculated using the standard Newtonian equation, (Equation 2),

$$D_F = 1/2 * \rho * v * C_d * A \tag{2}$$

where ρ is the mass density of the fluid, v the flow speed of the object relative to the fluid, and A is the reference area. For attaining higher speed velocities, reduction of the drag forces is pursued. Viscous drag contributes to the resistance forces that prevent the fish from having a better swimming speed.

II. MATERIALS AND METHODS

A. Algorithm for Generating the Caudal Fin

The algorithm for generating the caudal fin was created on the visual programming language software Grasshopper an add-in for Rhinoceros. A pseudorandom number generator (PRNG) was used for generating the parameters of the caudal fin. PRNG is an algorithm capable of generating a sequence of numbers that appears to have a random correlation between them. This algorithm is initialized with a seed that will determine the sequence of the numbers. Hence, the employment of different seeds will produce different sequences. However, the same sequence will be produced if the same seed is used.

The user can feed the program with the desired type of fin by control gates (Table III), and the PRNG will generate a number for each control point within a range (Table III). These control points are connected by curves to generate surfaces (see Fig. 2).

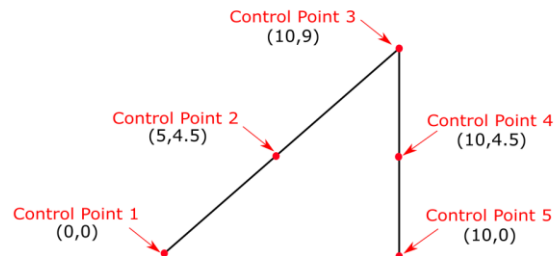


Figure 2. Control points and curves for generative design.

The range varies pseudo-randomly between two established numbers (see Table III). These numbers indicate the variation on their local coordinates. Even though the maximum range only has 4 units of difference, the pseudorandom number generated by the seed has up to 6 decimal places. By varying the thickness in the X axis different performance and efficiency of the BAUV [9], the performance is also affected.

TABLE III. GATES AND CONTROL POINTS

Shape	Gate	C. Point 1		C. Point 2		C. Point 3		C. Point 4		C. Point 5				
		X	Y	X	Y	X	Y	X	Y	X	Y			
Base	0	0	0	0	0	0	0	0	0	0	0			
Rounded	1	0	0	-2	-0	1	-2	-1	-0	1	-3	0		
Truncated	2	0	0	0	0	1	-2	0	-1	-1	-0	0		
Forked	3	0	0	0	0	0	-1	0	0	-4	-0	0		
Lunated	4	0	0	-2	-1	1	-4	0	-2	-1	-1	-6	-3	0

B. Computational Fluid Dynamics.

COMSOL Laminar Flow module was used to simulate the interaction of an array of five different caudal fins with three-dimensional models generated. The fin was considered as a solid, and the domain surrounding the fin was set as a fluid domain of water ($\rho=1000 \text{ kg/m}^3$). Fig. 3 and Table IV resume these parameters.

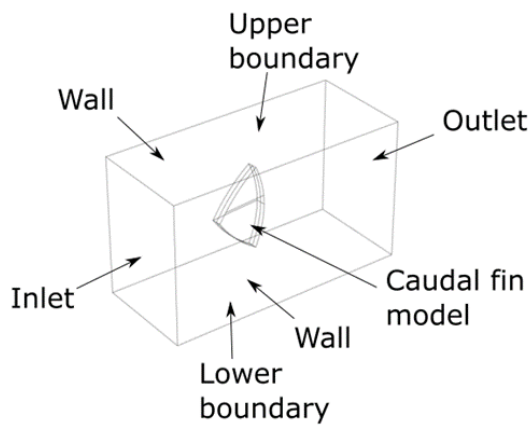


Figure 3. CFD Boundary conditions

TABLE IV. COMPUTATIONAL FLUID DYNAMICS PARAMETERS

	Type	Value
Inlet	Velocity inlet	5 [m/s]
Outlet	Pressure outlet	0 [Pa]
Upper and lower boundary	Wall	-
Wall	Wall	-
Caudal fin model	Wall	-

III. RESULTS AND DISCUSSION

Application parameters for the proposed methodology were applied using the parameters for gates and control points presented in Table V, a seed value 400 was

randomly settled. It should be noticed that using another number would produce similar but not identical models. As shown in the Figures (Fig. 4 and Fig. 5), these designs shown distinctive characteristics that resemble the shape of tails for distinctive swimming speeds of fishes.

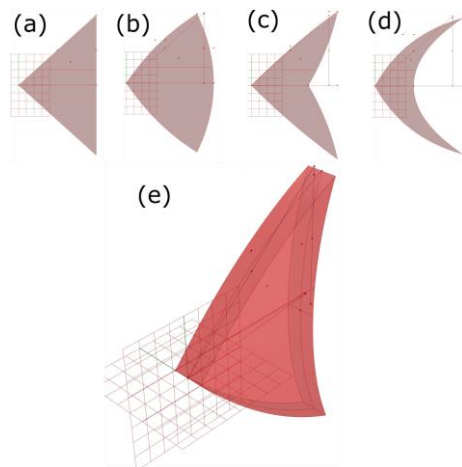


Figure 4. (a) Base model front view (b) Rounded model front view (c) Forked model front view (d) Lunated model front view (e) Truncated model isometric view.

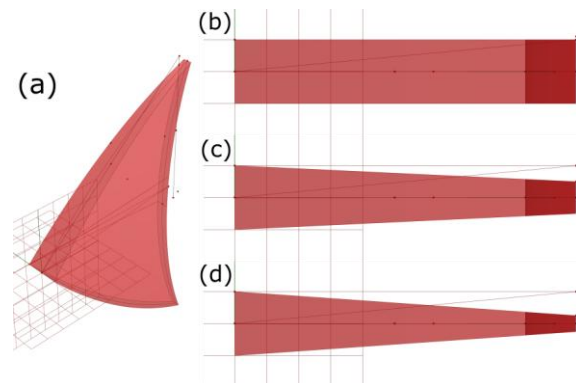


Figure 5. Truncated model (a) isometric view 25% trailing edge (b) top view 100% trailing edge (c) top view 50% trailing edge (d) top view 25% trailing edge.

TABLE V. GATES AND CONTROL POINTS FOR SEED 400

Shape	Gate	C. Point 1		C. Point 2		C. Point 3		C. Point 4		C. Point 5		Aspect Ratio
		X	Y	X	Y	X	Y	X	Y	X	Y	
Base	0	0	0	0	0	0	0	0	0	0	0	3.600
Rounded	1	0	0	-1.266	1.036	-0.880	-0.118	1.263	0	1.263	0	2.673
Truncated	2	0	0	0	1.263	0.666	-0.502	-0.916	0	-0.916	0	3.394
Forked	3	0	0	0	0.552	1.114	0.488	0	0	-2.662	0	4.445
Lunated	4	0	0	-1.418	2.124	1.334	-0.255	-5.017	0	-5.017	0	5.697

To evaluate the produced designs in terms of the hydrodynamic performance, we inspected the behavior of the caudal fins under a varying angle of attack (AoA) from 0° to 20° and plotted a surface plot of velocity magnitude at the plane of the foil (see Fig 6).

In Fig. 7 it can be shown the velocity magnitude with all the different models using all the AoA, and the streamlines of the fluid, however these results are only in $Y=0$, it important to clarify that it will vary depending on the Y axis.

Fig. 8 shows the mean velocity at the fin surface plane per AoA.

Fig. 9 shows the pressure distribution among the the models for the previously defined AoA. It should be noticed that these are only for $Y=0$. Therefore it will vary depending on the Y axis, as shown on the Fig. 10.

Fig. 10 shows an example of the calculated pressure distribution for a given AoA.

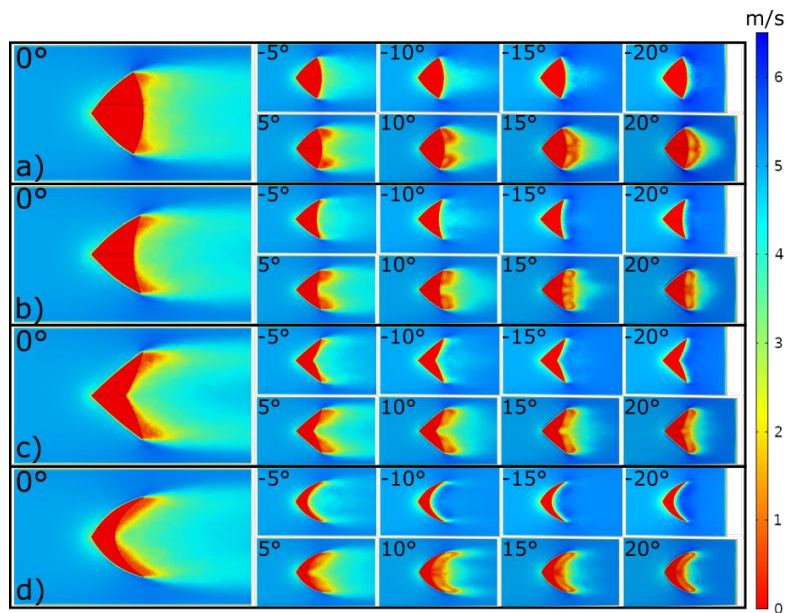


Figure 6. Velocity magnitude [m/s] slices at different angles (a) Rounded model (b) Truncated model (c) Forked model (d) Lunated model.

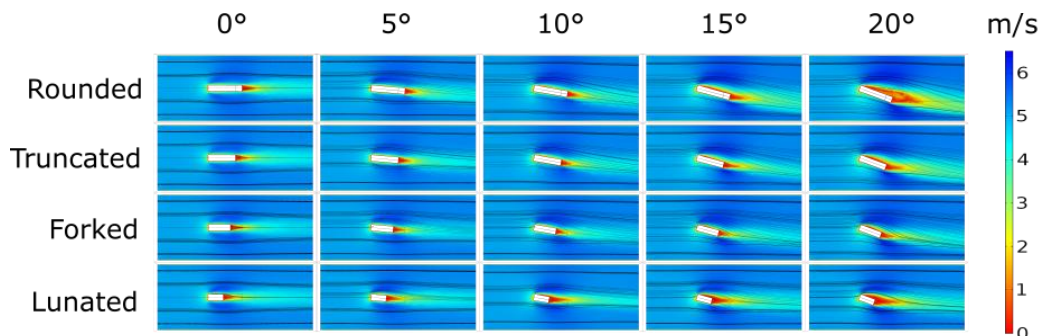


Figure 7. Velocity magnitude [m/s] top view comparison at $Y=0$.

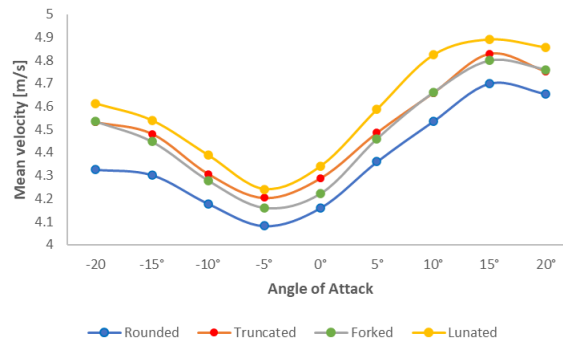


Figure 8. Mean velocity (m/s) vs AoA comparison.

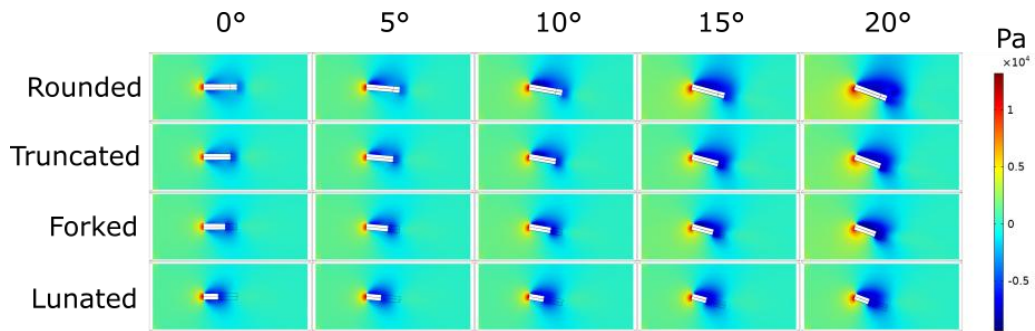


Figure 9. Fluid pressure (Pa) comparison at Y=0.

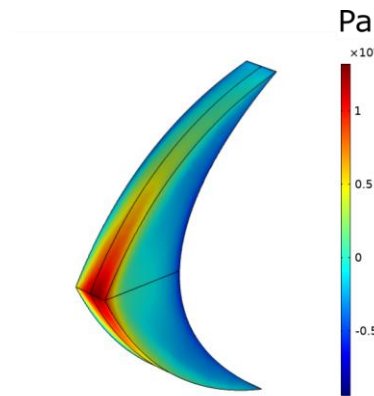


Figure 10. Pressure (Pa) distribution at Lunated model 15° α.

TABLE VI. ANGLE OF ATTACK VS DRAG COEFFICIENT C_D

Angle of Attack AoA	Rounded model	Truncated model	Forked model	Lunated model
0°	30.77 N	27.19 N	33.79 N	29.33 N
5°	34.73 N	29.6 N	36.16 N	30.48 N
10°	45.40 N	36.53 N	42.48 N	32.81 N
15°	59.07 N	45.81 N	51.36 N	37.61 N
20°	75.39 N	55.97 N	61.60 N	42.82 N
Increasing (max-min values) %	144.96	105.82	82.31	46.00

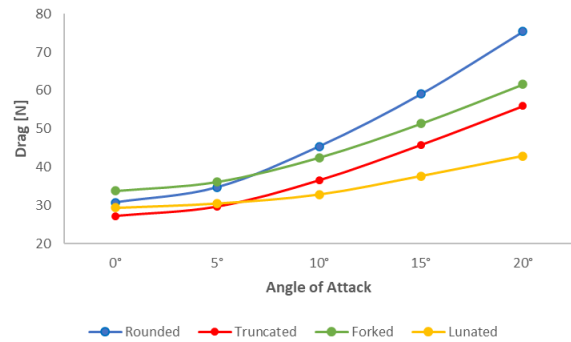


Figure 11. Angle of attack vs drag force (D_F).

In Table VI it can be shown how the drag generated is increasing proportionally as the angle of attack is increased. At 0°, the four models have almost the same value around 30.27. This amount is directly increased or reduced by the leading-edge shape and curve. The rate of the drag force increasing rates as shown in the Fig 11.

The last row of Table IV shows the increasing percentage between the AoA 0° and 20° of each model, while the values decrease from left to right, indicating that at a lower percentage the drag generated between the angle of attack variation will be lower and the fish speed will be higher as stated before (see Fig 1.).

It is observed that in the truncated model there is a lesser amount of drag compared to the forked model. This behaviour is caused by the greater curvature at the leading edge of the truncated model (see Fig. 4b and 4c) The longer fin span modifies a larger model area (see Table V, Control Point 3). As the AoA increases, there is a greater increase. This can be seen in the percentage of increase between angle of attack 0° and 20°.

From Eq. 2 it was able to obtain the Table VII using the frontal area of each caudal fin as the area A and the parameters used to solve the computational fluid dynamics analyses. These values are dimensionless and provided means to benchmark the performance among different design under different conditions.

Fig. 12 shows how the AoA affects increase is associated with a Cd increase. The forked model showed a better performance compared to the truncated model as it has a lower increase in its Cd while the AoA increases in such a way that when it reaches 20° it has a lower Cd even when it started with a bigger Cd at 0°.

Data suggests that the Cd at angle of attack 0° is mainly influenced by the curvature of the leading edge and the size of the fish span on this 4 models, however as the AoA increases, the shape of the model influences on the Cd and the drag.

TABLE VII. ANGLE OF ATTACK VS DRAG COEFFICIENT C_D

Angle of Attack AoA	Rounded model	Truncated model	Forked model	Lunated model
0°	0.69	0.64	0.71	0.67
5°	0.78	0.69	0.76	0.69
10°	1.02	0.85	0.89	0.75
15°	1.33	1.07	1.08	0.86
20°	1.69	1.31	1.29	0.97
Area [mm ²]	3553	3399	3795	3498

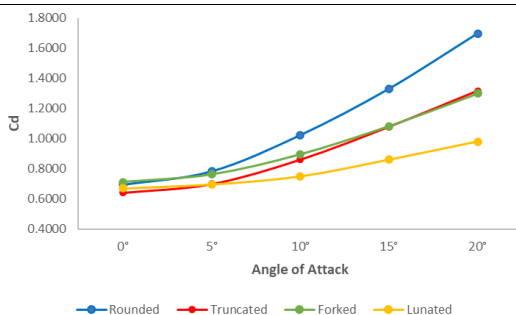


Figure 12. Angle of Attack vs Drag coefficient (Cd).

IV. CONCLUSIONS

This work shows that development of a caudal fin CAD design is possible using of visual programming language. The methodology employs controlled curves by predefined control points that can be changed for generation of distinctive shapes.

Parametric modeling is a reliable tool for creation of 3D models, because allows tweaking the features by modifying an initial parameter. While it may be necessary to invest time coding in VPL, time can be saved later from the possibility of mimicking a natural feature from scratch without redrawing the model. This feature, for example, could be implemented with genetic algorithms towards optimization.

For future work it will be desired to work with transient flow analysis, for better results, including not only discrete stationary angles but all the range between them. Moreover, more features on the design could enhance the flexibility of the proposed methodology. Furthermore, work remains to be developed to test this concept with additive manufacturing and experimental testing for fishes and other types of animals.

CONFLICT OF INTEREST

The authors declare no conflict of interest.

AUTHOR CONTRIBUTIONS

Biali Fernando and JIML contributed with the conceptualization, investigation, and Methodology. Edison Naula supported the software and visualization. Ciro Rodriguez supported the funding acquisition, project management and conceptualization. The original draft was generated by Biali Fernando, and the review and editing and overall supervision of the project was executed by J. Israel Martínez-Lopez.

ACKNOWLEDGMENT

The Research Group of Advanced Manufacturing from Tecnológico de Monterrey provided support for acquiring materials and goods. The authors acknowledge the support provided from the Laboratorio Nacional de Manufactura Aditiva y Digital (MADiT).

REFERENCES

- [1] ASTM International, F2792-12a - Standard Terminology for Additive Manufacturing Technologies. 2013.
- [2] N. Guo and M. C. Leu, "Additive manufacturing: Technology, applications and research needs," *Front. Mech. Eng.*, vol. 8, no. 3, pp. 215–243, 2013.
- [3] D. S. Thomas and S. W. Gilbert, "Costs and cost effectiveness of additive manufacturing," *NIST Spec. Publ.*, vol. 1176, p. 12, 2014.
- [4] S. H. Huang, P. Liu, A. Mokasdar, and L. Hou, "Additive manufacturing and its societal impact: A literature review," *International Journal of Advanced Manufacturing Technology*, 2013.
- [5] J. Allen, "An investigation into the comparative costs of additive manufacture vs. machine from solid for aero engine parts," *Cost Eff. Manuf. via Net-Shape Process.*, 2006.
- [6] C. Bal, G. Ozmen Koca, D. Korkmaz, Z. H. Akpolat, and M. Ay, "CPG-based autonomous swimming control for multi-tasks of a biomimetic robotic fish," *Ocean Eng.*, 2019.

- [7] M. Sfakiotakis, D. M. Lane, and J. B. C. Davies, "Fish Swimming Techniques," *J. Ocean. Eng.*, vol. 24, no. 2, pp. 237–252, 1999.
- [8] A. Apalkov, R. Fernández, J. G. Fontaine, T. Akinfiyev, and M. Armada, "Mechanical actuator for biomimetic propulsion and the effect of the caudal fin elasticity on the swimming performance," *Sensors Actuators, A Phys.*, vol. 178, pp. 164–174, 2012.
- [9] S. Heo, T. Wiguna, H. C. Park, and N. S. Goo, "Effect of an artificial caudal fin on the performance of a biomimetic fish robot propelled by piezoelectric actuators," *J. Bionic Eng.*, vol. 4, no. 3, pp. 151–158, 2007.
- [10] L. Junqiang, Y. Yiling, W. Chuanyu, L. Guoping, C. Tehuan, and M. Jianqiang, "Underwater oscillation performance and 3D vortex distribution generated by miniature caudal fin-like propulsion with macro fiber composite actuation," *Sensors Actuators, A Phys.*, vol. 303, p. 111587, 2020.
- [11] T. Salumäe and M. Kruusmaa, "A flexible fin with bio-inspired stiffness profile and geometry," *J. Bionic Eng.*, vol. 8, no. 4, pp. 418–428, 2011.
- [12] T. Wang, L. Wen, J. Liang, and G. Wu, "Fuzzy vorticity control of a biomimetic robotic fish using a flapping lunate tail," *J. Bionic Eng.*, vol. 7, no. 1, pp. 56–65, 2010.
- [13] P. Riggs, A. Bowyer, and J. Vincent, "Advantages of a biomimetic stiffness profile in pitching flexible fin propulsion," *J. Bionic Eng.*, vol. 7, no. 2, pp. 113–119, 2010.
- [14] A. D. Marchese, C. D. Onal, and D. Rus, "Autonomous soft robotic fish capable of escape maneuvers using fluidic elastomer actuators," *Soft Robot*, vol. 1, no. 1, pp. 75–87, 2014.
- [15] M. Ay, D. Korkmaz, G. O. Koca, C. Bal, Z. H. Akpolat, and M. C. Bingol, "Mechatronic design and manufacturing of the intelligent robotic fish for bio-inspired swimming modes," *Electron*, vol. 7, no. 7, 2018.
- [16] C. T. Aparicio-García, E. A. N. Duchi, L. E. Garza-Castañón, A. Vargas-Martínez, J. I. Martínez-López, and L. I. Minchala-Ávila, "Design, construction, and modeling of a BAUV with propulsion system based on a parallel mechanism for the caudal fin," *Appl. Sci.*, 2020.
- [17] A. Krishnadas, S. Ravichandran, and P. Rajagopal, "Analysis of biomimetic caudal fin shapes for optimum propulsive efficiency," *Ocean Eng.*, vol. 153, no. December 2017, pp. 132–142, 2018.



Biali F. Lima Rodríguez is an aeronautical engineer from Universidad Autónoma de Nuevo León, Monterrey, México. Currently he is pursuing a M.Sc. in Manufacturing Systems at Tecnológico de Monterrey, Monterrey, México. His research interests are mainly in the areas of FEA, CAD modeling and 3D printing.



Edisson A. Naula Duchi obtained a B.S. in Electronic and Telecommunications Engineering from the University of Cuenca (2017) and a M.S. degree in Engineering Sciences from Tecnológico de Monterrey (2019). He is currently a full-time student of Ph.D. in Nanotechnology program in ITESM Campus Monterrey.



Ciro A. Rodríguez holds a B.S. in Mechanical Engineering from The University of Texas at Austin (1989) and a Ph.D. from The Ohio State University (1997). He worked in the automotive and machine tool industry. He is Visiting Scientist at the Osteoengineering Lab of The Ohio State University (2016 to 2018). He is currently Professor at the Department of Mechanical Engineering and Advances Materials at Tecnológico de Monterrey. He leads the research group in Advanced Manufacturing.



J. Israel Martínez López holds the Ph.D. and M.S. degrees in Science Engineering and Biotechnology from Tecnológico de Monterrey. He has worked in designing and testing microfluidic devices and collaborated at the Massachusetts Institute of Technology asat the Jongyoon Han Group. He is currently a research professor at the Tecnológico de Monterrey, where he leads research in Point-of-Care devices and Bioengineering

Copyright © 2022 by the authors. This is an open access article distributed under the Creative Commons Attribution License ([CC BY-NC-ND 4.0](https://creativecommons.org/licenses/by-nc-nd/4.0/)), which permits use, distribution and reproduction in any medium, provided that the article is properly cited, the use is non-commercial and no modifications or adaptations are made.